

See discussions, stats, and author profiles for this publication at: <https://www.researchgate.net/publication/272137318>

Influence of Zirconium Addition in Platinum–Hexagonal Mesoporous Silica (Pt–HMS) Catalysts for Reforming of n -Heptane

ARTICLE in INDUSTRIAL & ENGINEERING CHEMISTRY RESEARCH · SEPTEMBER 2014

Impact Factor: 2.59 · DOI: 10.1021/ie5024244

CITATION

1

READS

23

3 AUTHORS, INCLUDING:



Mohammad Hassan Peyrovi

Shahid Beheshti University

24 PUBLICATIONS 208 CITATIONS

[SEE PROFILE](#)



Nastaran Parsafard

Shahid Beheshti University

12 PUBLICATIONS 16 CITATIONS

[SEE PROFILE](#)

Influence of Zirconium Addition in Platinum–Hexagonal Mesoporous Silica (Pt-HMS) Catalysts for Reforming of *n*-Heptane

Mohammad H. Peyrovi,* Nastaran Parsafard, and Parnian Peyrovi

Department of Physical Chemistry, Faculty of Chemistry, University of Shahid Beheshti, Tehran 1983963113, Iran

ABSTRACT: A series of platinum/zirconium–hexagonal mesoporous silica (Pt/Zr-HMS) catalysts with different molar ratios of Si/Zr have been prepared and used for reforming reaction. The prepared catalysts were characterized by XRD, XRF, NH₃-TPD, FTIR, Py-IR, nitrogen sorption, SEM, and TGA (for studying the coke deposition) techniques. The effects of various amounts of zirconium on the activity, selectivity, and coke deposition in the temperature range of 200–500 °C were compared. By increasing the incorporation of Zr into the Pt-HMS structure, the acidity of catalysts increased. The results show that the catalytic activity and selectivity for desired products (especially isomerization products) increased with decreasing Si/Zr amount (or increasing zirconium content). The best i-C₇ selectivity (64.1%) was observed for Zr(5)-HMS at $T = 200$ °C.

INTRODUCTION

Naphtha is one of the petroleum fractions that consists of a complex mixture of hydrocarbon molecules generally having 5–12 carbon atoms. Naphtha is used mainly as feedstock for producing high-octane gasoline. Despite many efforts to raise the octane number of gasoline, the oil industry is under increasing pressure from legislatures to improve the quality of gasoline fuels and reduce exhaust emissions of greenhouse gases and air pollutants. To raise the octane number, one of the most important and economical catalytic processes in the petroleum refining industry is the isomerization of *n*-alkanes to *i*-alkanes. In this process, the straight-chain alkanes are transformed into branched isomers, improving research octane number (RON) to improve gasoline fuel quality.¹ It is well-known that this process is usually carried out on a bifunctional catalyst, consisting of a protonating acid and a metal function. According to the traditional mechanism, the noble metal catalyzes hydrogen transfer reactions (hydrogenation/dehydrogenation), whereas the isomerization and cracking of the hydrocarbon skeletons are performed on Brønsted acid sites.¹ It is essential for the selective conversion of alkanes into desirable products that the molecular transfers between the metal and acid sites take place rapidly, so a good balance between the metal and acid sites will obtain a suitable catalyst for this process.²

Recent research studies have been focused on mesoporous molecular sieves for comparable or improved catalytic properties in various reactions. The mesoporous materials have high surface area, uniform and size-controllable pore structure, and Si exchangeable by other elements,³ but the silica surface of these materials has weak reactivity. This weak reactivity is related to surface silanol groups capable of forming only hydrogen bonds with foreign gaseous molecules or hardly ionizing in aqueous solutions.⁴ To improve the acid and/or redox properties of these materials, various metals, such as Al,^{5,6} Fe,⁷ Mn,⁸ V,^{7,9} Co,¹⁰ Ti^{11–14} and Zr,^{14,15} have been added to mesoporous frameworks.

Zirconium oxide (ZrO₂), known as zirconia, is also a relevant material in adsorption and catalysis. Zirconia is a special transition metal oxide that possesses not only weak acid and

base properties but also redox activities and high ion-exchange capacity. Therefore, it is widely used in catalytic processes as a catalyst, support, and promoter.^{3,16,17} Pure zirconia supports have relatively small surface area and irregular pore size, which may limit their potential application for catalyzing large molecules and decrease active sites.¹⁸ Whereas zirconium-doped mesoporous silica displays strong acidity, the acidities of both zirconia and silica are weak.³

In a previous work, our group investigated the catalytic activities of Pt catalysts supported on aluminum–hexagonal mesoporous silica (Al-HMS) for *n*-heptane reforming.⁵ In the present study Pt supported on HMS and Zr-HMS have been explored as reforming catalysts. *n*-Heptane was used as one of the hydrocarbons in naphtha. To our knowledge, no published work has been reported using Pt/Zr-HMS catalyst with various amounts of zirconium for reforming of *n*-heptane. Thus, the purpose of this work is to study the catalyst activity, selectivity, coke formation, RON, and kinetics of this catalytic reaction at a temperature range of 200–500 °C. Even though the reforming reaction is used in a high-temperature range, to investigate the isomerization products, we also examine the low-temperature range.

EXPERIMENTAL SECTION

Materials and Procedures. The HMS and Zr-HMS materials were synthesized by using a sol–gel method similar to those of Tannev and Pinnavaia¹⁹ and also Kostova et al.,²⁰ who used tetraethyl orthosilicate (TEOS) as a silica source, zirconyl nitrate (ZrO(NO₃)₂·8H₂O) as a zirconium source, and dodecylamine as a surfactant. The samples of various Si/Zr ratios were obtained by taking appropriate amounts of zirconyl nitrate and TEOS for Si/Zr ratios of 5, 10, 20, and 35. The solid products were separated by filtration and dried at 110 °C overnight and calcined at 600 °C for 6 h in air. Moreover, Pt

Received: June 17, 2014

Revised: August 15, 2014

Accepted: August 26, 2014

Published: August 26, 2014



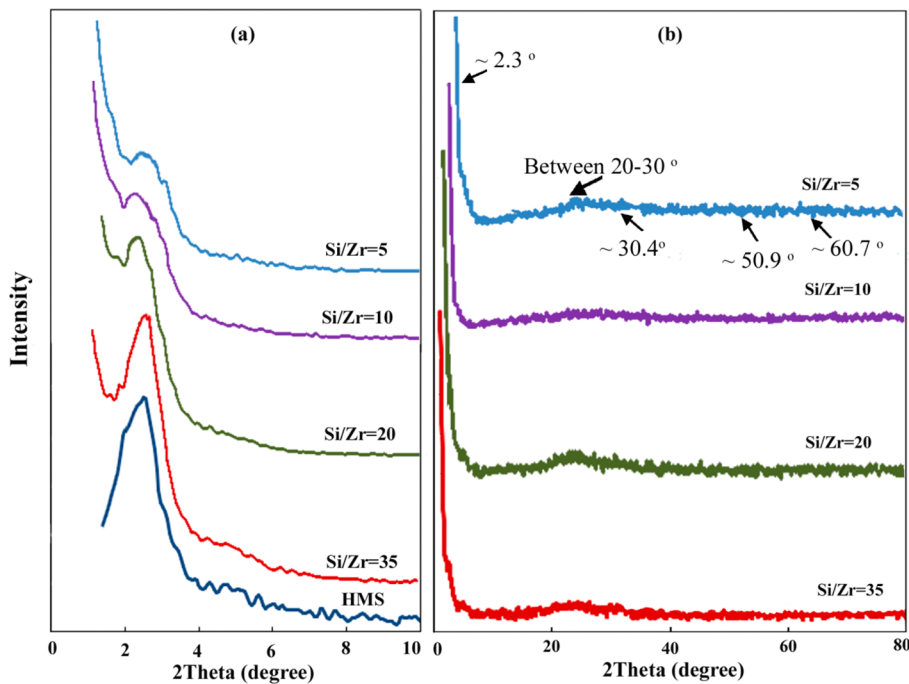


Figure 1. (a) Low- and (b) high-angle XRD patterns of the synthesized catalysts.

(0.6 wt %) catalysts were prepared by impregnating the supports (HMS and Zr(α)-HMS) with an appropriate concentration of H_2PtCl_6 . After evaporation of the solvent and drying, the calcination of platinated catalysts was done in air and at 300 °C for 4 h. These catalysts were designated Pt/Zr(α)-HMS, α being the Si/Zr amount. In addition, to compare, we synthesized a Pt/Al-HMS catalyst using a method similar to that described method in our previous work.⁵ It should be noted that all materials were purchased from Merck Co. and were used as received without any further purification.

Characterization Methods. The X-ray diffraction (XRD) patterns were obtained from an X-PERT diffractometer operated at 45 kV and 50 mA utilizing Ni-filtered Cu $K\alpha$ radiation. Data were collected within a 2θ range of 1°–80° with a 0.06° 2θ step and 1 s per step. For measuring Si/Zr content in our synthesized catalysts, we used XRF (XRF-8410 Rh 60 kV). N_2 adsorption–desorption results were obtained at –196 °C by an ASAP-2010 micromeritics (USA) instrument. The temperature was kept constant by liquid nitrogen. Specific surface area (S_{BET}) was evaluated by the BET equation applied to the relative pressures (P/P_0) between 0.05 and 0.30. The average pore diameter was evaluated by applying the Barret–Joyner–Halenda method (BJH) to the adsorption branches of the N_2 isotherms. The cumulative pore volume was attained from the isotherms at $P/P_0 = 0.99$. The acidity of Zr(α)-HMS catalysts was calculated by temperature-programmed desorption of NH_3 (NH_3 -TPD) in a TPD/TPR analyzer (2900 Micromeritics) equipped with a TCD. Catalysts were activated at 500 °C for 1 h in a flow of helium; then, ammonia was introduced by a He stream containing 10 (vol) % of ammonia at 100 °C. The physically adsorbed NH_3 was removed by purging with a helium flow at 100 °C until the baseline was flat. Then the reactor temperature was ramped at a rate of 10 °C/min. The NH_3 -TPD desorption profiles of pretreated catalysts were recorded from 25 to 300 °C. For evaluating and analyzing the type of acidic sites, pyridine adsorption (Py-IR) on the catalysts was carried out with a Fourier-transform infrared

spectrometer (170-SX). Self-supported wafers of the samples with a weight/surface ratio of about 12 mg cm^{–2} were placed in a vacuum cell with greaseless stopcocks and CaF₂ windows. The samples were evacuated at 250 °C and 10^{–2} Pa overnight, exposed to pyridine vapors at room temperature for 30 min, and then outgassed at 200 °C. The dispersion of platinum on Zr(α)-HMS materials was evaluated by the hydrogen adsorption method in a TPD/TPR analyzer. The platinated catalysts were evacuated at 500 °C for 1 h and then reduced with hydrogen at 450 °C for 1 h and evacuated at the same temperature for 1 h before hydrogen adsorption. The amount of coke laid down on the catalyst surface was measured by thermogravimetric analysis (TGA) equipment using an STA503 M instrument. This analysis was carried out with a heating rate of 10 °C/min in a temperature range of 25–800 °C and in flowing air. In addition, to show the morphology of catalyst, field emission scanning electron microscopy (FESEM) was performed with a Hitachi S-4160 scanning electron microscope with an accelerating voltage of 30 kV.

Catalytic Assessment. The *n*-heptane (*n*-C₇) reforming in the flowing hydrogen was carried out at 200–500 °C and $P = 1$ atm in a continuous fixed-bed microreactor packed with 1.0 g of catalyst. The bed temperature was maintained constant within ±1 °C as measured with a K-type thermocouple traveling along the bed axis. The catalysts were pretreated at 450 °C for 2 h in the flowing hydrogen (40 mL min^{–1}). The liquid reactant (*n*-C₇) was fed into a reactor with space velocity (LHSV) 2.0 h^{–1}. Hydrogen was also introduced in an optimized amount of H₂/C₇ molar ratio for our samples to obtain the best selectivity of desired products (H₂/HC = 7). The performance of catalysts was tested after 1 h of time on stream (TOS) at noted temperatures for each experiment. The catalytic performance was also investigated at 400 °C for 6 and 100 h TOS, and the reaction products were analyzed by an online gas chromatograph (Agilent Technologies 7890A) equipped with an FID.

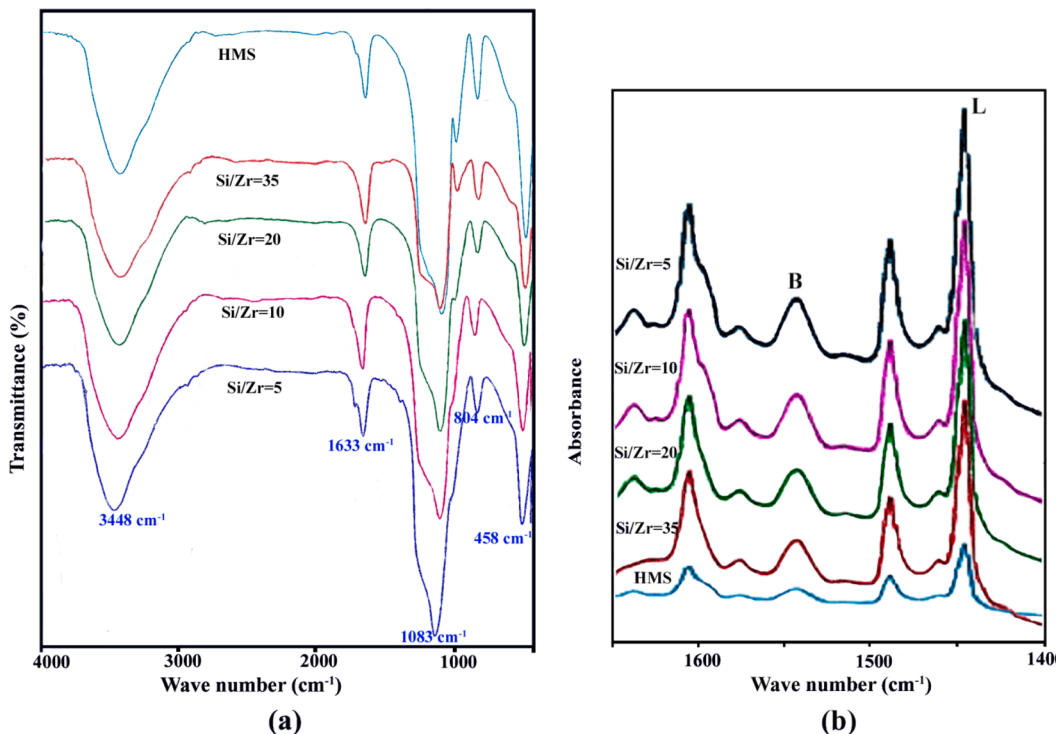


Figure 2. (a) FT-IR spectra of KBr pellets; (b) IR spectra of adsorbed pyridine for different samples.

RESULTS AND DISCUSSION

Characterization. The crystallinity of the calcined catalysts was studied by the powder XRD patterns at low (Figure 1a) and high angles (Figure 1b). All materials showed a reflection at small angles ($2\theta \sim 2.3^\circ$) that is characteristic of HMS⁵ and can be assigned to a lattice with a short-range hexagonal symmetry. There is also a broad diffraction line between 20° and 30° , which was attributed to the amorphous part of the substrate. A set of peaks near 30.4, 50.9, and 60.7 presents the formation of tetragonal zirconia, but these reflections have low intensity and the peaks cannot be seen clearly. The low intensity of these reflections shows the presence of a highly dispersed zirconia phase and the absence of the genesis of large discrete ZrO_2 crystallites.²¹ The increase of zirconium content results in decreasing HMS peak intensity and broadening of this peak, indicating that incorporation of zirconium is associated with increasing lattice disorder.

Figure 2a shows the infrared spectra for HMS and $\text{Zr}(x)$ -HMS catalysts. The IR spectra recorded at room temperature show a broad absorption band covering the region between 3700 and 3000 cm^{-1} , which is due to water adsorbed on the sample surface.²² Also, the samples present a slender but distinct vibration near 1635 cm^{-1} , which is characteristic of the hydroxyl flexion vibration of water adsorbed on the molecular sieve samples. This band is seen in all sample spectra. In addition, it shows distinct absorptions near 1230 , 1080 , and 452 cm^{-1} , which are assigned to the asymmetric stretching and $\equiv\text{Si}-\text{O}-\text{Si}\equiv$ bending modes of HMS. The absorption bands near 459 , 573 , 795 , 961 , and $1260-1000\text{ cm}^{-1}$ show asymmetric $\text{Si}-\text{O}-\text{Si}$ stretching, $\text{Si}-\text{O}-\text{Si}$ bending, $\text{Si}-\text{O}-\text{Si}$ deformation, symmetric $\text{Si}-\text{O}-\text{Si}$ stretching, and $\text{Si}-\text{OH}$ rocking, respectively. After incorporation of Zr, the $\text{Si}-\text{OH}$ rocking peak at 961 cm^{-1} shifted to lower wave numbers and broadened, suggesting interaction between the surface silanol groups with neighboring Zr cations. Furthermore, the $\text{Si}-\text{O}$

stretching in $\text{Si}-\text{O}-\text{Zr}$ heterolinkages appeared as a weak shoulder peak at 907 cm^{-1} . No absorption band corresponding to zirconium phase was found in FT-IR spectra, so it shows that Zr was highly dispersed.³

Typical SEM photographs are given in Figure 3. SEM photographs show that the catalysts after the zirconium loading have the same morphology, which corresponds to aggregates without regular shapes. Moreover, small spherical structures are seen in these images that represent the presence of HMS. It should be noted that because the SEM photographs for these catalysts are the same, only SEM photographs of $\text{Zr}(5)$ -HMS with various dimensions are shown.

The textural properties of these porous materials were determined by the physical adsorption of nitrogen. The adsorption–desorption behaviors of these materials have similar characters. Table 1 shows BET surface areas of mesopores (S_{meso}) and volumes of mesopores (V_{meso}). As can be seen, all supports show the high BET surface areas. The specific surface area of the prepared materials and pore volume decrease with increasing zirconium content. This is due to the fact that at high zirconium content, some of the mesopores are probably collapsed and large pores are formed from the internanoparticle boundaries, leading to reduced pore volume and surface area.

In this table, the total amounts of desorbed ammonia are reported. The IR spectra of pyridine adsorbed on HMS and $\text{Zr}(x)$ -HMS were taken to investigate the nature of the acid sites. Figure 2b shows the Py-IR spectra of HMS and $\text{Zr}(x)$ -HMS samples after adsorption of pyridine and desorption at room temperature. According to the area ratio, we can say that the number of Lewis acidic sites was greater than that of Brønsted sites. It is well-known that the vibration bands in the $1400-1650\text{ cm}^{-1}$ regions of the Py-IR spectrum could distinguish between the Brønsted and Lewis acid sites.^{23,24} Lewis acidic sites are characterized at 1450 and 1609 cm^{-1} , and

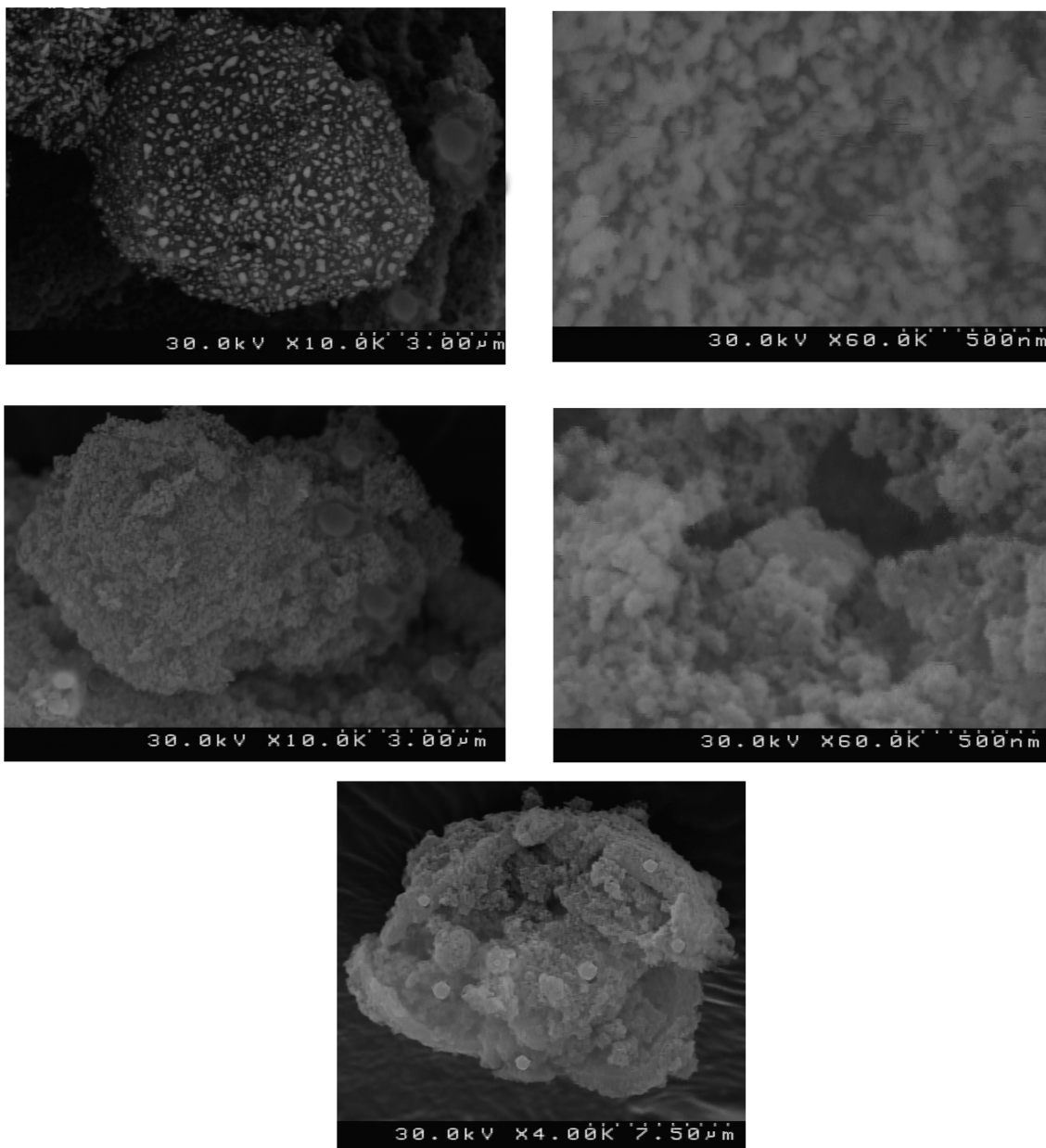


Figure 3. Typical SEM photographs of Zr(5)-HMS sample.

Table 1. Textural Data Obtained from N₂ Adsorption–Desorption Isotherms and H₂ Chemisorption

catalyst	Si/Zr	S_{BET} (m^2g^{-1})	S_{meso} (m^2g^{-1})	V_{meso} (cm^3g^{-1})	D_p^a (nm)	acidity using NH ₃ (mmol/g)	M_d^b
HMS		818	570	0.51	4.5	0.110	78
Zr(5)-HMS	4.8	808	594	0.47	3.3	0.376	76
Zr(10)-HMS	9.2	820	601	0.54	2.8	0.372	79
Zr(20)-HMS	18.1	844	616	0.69	2.5	0.364	80
Zr(35)-HMS	34.7	880	639	0.92	2.3	0.352	83

^aPore diameter. ^bMetal dispersion (%).

Brønsted acidic sites are detected at ca. 1550 cm^{-1} .²¹ Also, the peak near 1480 cm^{-1} corresponded to Lewis and Brønsted (L + B) sites.²⁵ As can be seen, the band intensities for adsorbed pyridine on Brønsted and Lewis acid sites increase with increasing amount of Zr. The acid properties of these catalysts are presented using the Brønsted acid to Lewis acid ratio from their specific bands, namely, an IR band at 1550 cm^{-1} for Brønsted acid and an IR band at 1609 cm^{-1} for Lewis acid.²⁵

TPD results show two overlapping peaks that have temperature maxima near 88 and 119 °C (not shown here). This shows that the acidic sites of all samples are not strong. As can be seen, the total acidity increases with increasing Zr amount. According to these results and the results of the pyridine-IR spectroscopy, the most acidic sites on Zr-HMS catalyst are Lewis type.

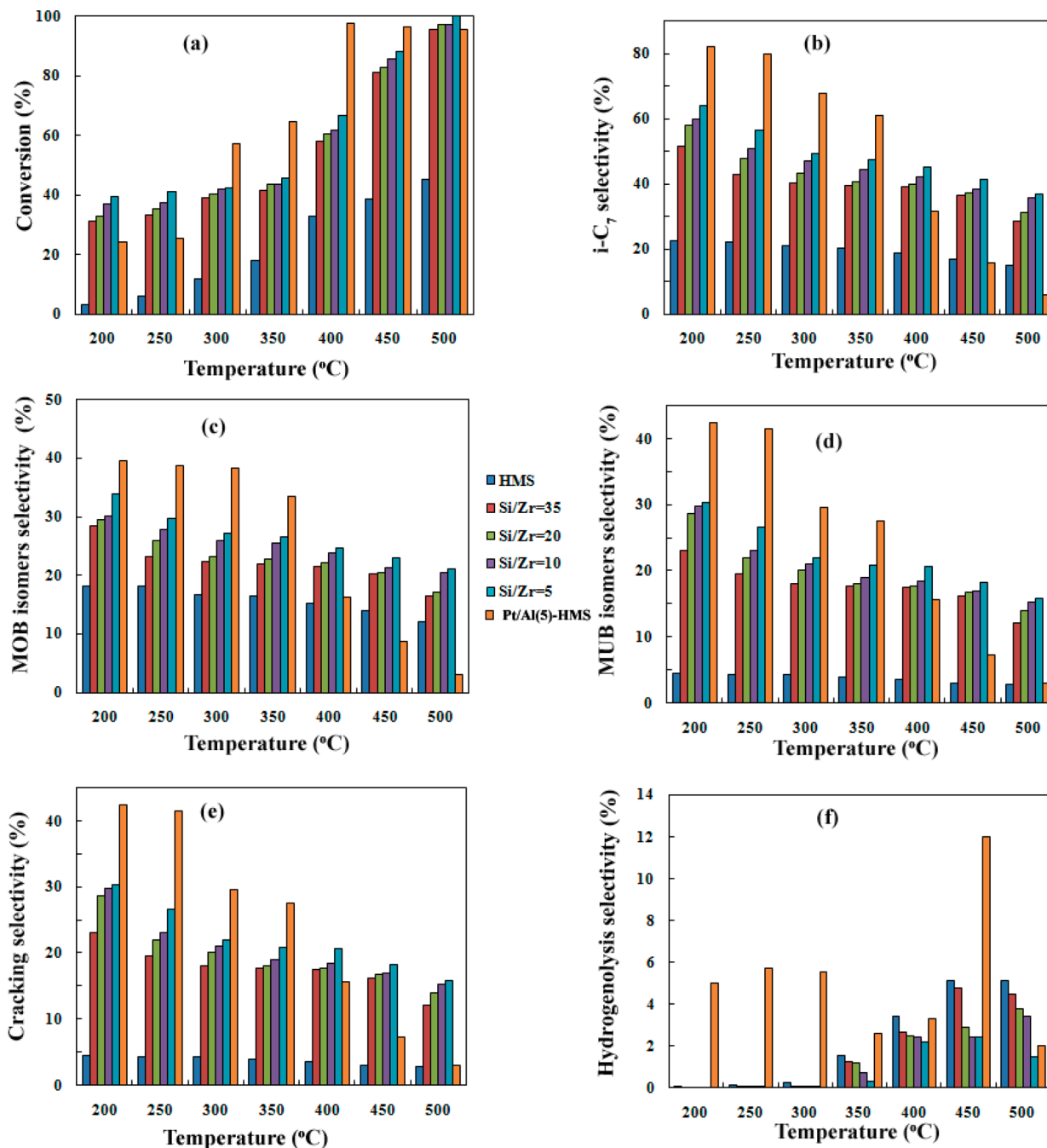


Figure 4. (a) n-C₇ conversion; selectivity for (b) MON + MUB isomers; (c) MOB isomers; (d) MUB isomers; (e) cracking and (f) hydrogenolysis products over Pt/HMS, Pt/Zr(x)-HMS, and Pt/Al(5)-HMS catalysts at various temperatures.

Catalytic Performance of n-C₇. The experimental data have been measured on Pt-loaded HMS and Zr ($x = 5, 10, 20$, and 35)-HMS. The conversion and selectivity of products are defined as follows:

$$\text{conversion} = \% \text{ of n-C}_7 \text{ transformed into products} \quad (1)$$

$$\text{selectivity} = \frac{\% \text{ of n-C}_7 \text{ transformed into a certain product}}{\text{total amount of n-C}_7 \text{ converted}} \quad (2)$$

The catalyst activities were evaluated by reforming of n-C₇ over these catalysts between 200 and 500 °C. Pt/Zr(x)-HMS catalysts as compared with Pt/HMS are highly active for n-C₇ conversion (Figure 4a). Increasing the reaction temperature to

500 °C increased almost linearly n-C₇ conversion. As can be seen, the highest conversion was obtained for Pt/Zr(5)-HMS catalyst. As might be expected, the catalytic activity follows the surface acidity variation (Table 1).

A question arises as to whether the conversion is determined by the activity of catalyst itself (kinetic regime) or is limited by transport phenomena (diffusion regime), so prior to other studies, we investigated the reaction kinetics and the mass transfer limitation effect during the reaction.

The Koros–Nowak²⁶ and Madon–Boudart^{27,28} tests can be used to investigate the mass transfer limitations. According to these tests, in the absence of all transport limitations, the rate of a reaction is proportional to the number of active sites, which in turn is proportional to the catalyst weight. Therefore, we

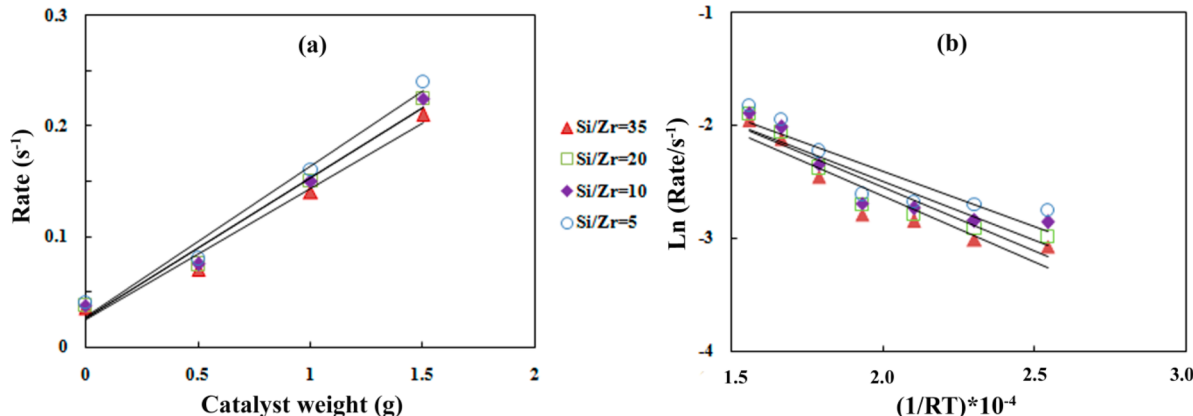


Figure 5. (a) Effect of catalyst weight on the reforming rate of $n\text{-C}_7$ at 773 K temperature; (b) Arrhenius plot.

Table 2. TOF Data and Activation Energies for Reforming Reaction on Various Catalysts

temp (°C)	TOF ^a (h ⁻¹)			
	Pt/Zr(5)-HMS	Pt/Zr(10)-HMS	Pt/Zr(20)-HMS	Pt/Zr(35)-HMS
200	230	206	181	167
250	240	209	194	176
300	246	234	222	209
350	265	244	241	221
400	388	346	335	309
450	512	479	458	432
500	581	545	537	508

E_a^b (kJ/mol) 9.8 10.3 11.3 11.6

^aTurnover frequency = $[(Q\rho)/M \times N_A \times \text{conversion}] / [(m_{\text{cata}} \times \% \text{ metal})/(M_{\text{metal}})] \times N_A \times \text{dispersion}$, where Q = volumetric flow rate of $n\text{-C}_7$ (2 cm³/h), ρ = density of $n\text{-C}_7$, M = molecular weight of $n\text{-C}_7$, m_{cata} = mass of catalyst; % metal = metal dispersion (%); N_A = Avogadro's constant. ^bFrom Arrhenius plot.

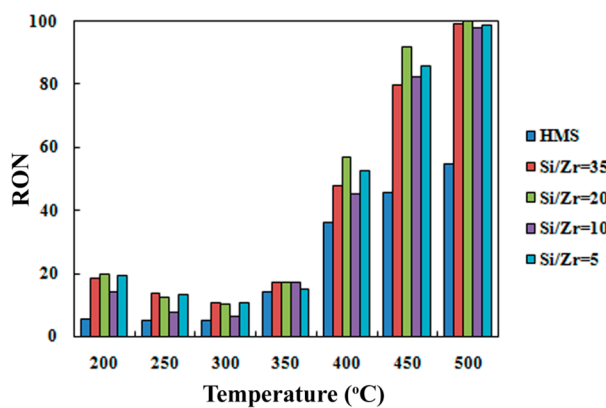


Figure 6. RON versus temperature for various catalysts.

prepared a mixture of each catalyst with an inert powder and measured those reaction rates. The plot of rate (TOF) versus the catalyst weight is linear and the rate increased proportionally with the weight of catalyst (Figure 5a), indicating the absence of any mass transfer limitations during the reaction.²⁹ Thus, the rate of $n\text{-C}_7$ conversion under these conditions is controlled by the intrinsic reaction kinetics and is free from transport limitations.

Figure 5b shows Arrhenius plots for Pt/Zr(x)-HMS catalysts. Pt/Zr-HMS catalyst with a Si/Zr ratio of 5 has the highest turnover frequency (TOF) and an activation energy of 9.8 kJ mol⁻¹ for $n\text{-C}_7$ reforming. Increasing the Si/Zr ratio decreased the TOF and increased the activation energy (Table 2). Due to the smaller activation barrier on Pt/Zr(5)-HMS than on other catalysts, the reaction on this catalyst will be facile, and so the $n\text{-C}_7$ conversion will be very good.

In Figure 4, we have also shown the selectivity of mono-, multi-, and (mono + multi)-branched heptanes (denoted MOB, MUB, and MOB + MUB, respectively), cracking and hydrogenolysis products against the reaction temperatures. It has been well demonstrated that the conversion of $n\text{-C}_7$ into isoheptanes ($i\text{-C}_7$) increased with decreasing temperature. Due to the thermodynamic limitation of the isomerization reaction, the selectivity of $i\text{-C}_7$ decreases with increasing temperature. The acidity, geometry of pores, and platinum dispersion are factors that affect the isomerization reaction on mesoporous catalysts. To illustrate the effect of these parameters, Wang et al.¹ used an isomerization selectivity parameter (S_p). Factors related to reaction conditions and to the catalyst are two groups of effective factors on the isomerization.

$$S_p = S_{\text{selectivity parameter}} = F_{\text{catalyst}} F_{\text{reaction conditions}} \quad (3)$$

$F_{\text{reaction conditions}}$ is a function of reaction temperature, pressure, space velocity, reaction time, and etc. Because the reaction conditions are constant in all experiments, S_p depends only on the catalyst parameters:

$$F_{\text{catalyst}} = f_{\text{acidity}} f_{\text{metal}} f_{\text{geometry}} \quad (4)$$

f_{acidity} is defined as the Brønsted acid density, f_{metal} is related to the metal dispersion, and f_{geometry} is simply defined as the pore diameter of the catalyst. We define the isomerization selectivity parameter of support (S_{ps}) as

$$S_{ps} = f_{\text{acidity}} f_{\text{geometry}} \quad (5)$$

Consequently

$$S_p = S_{ps} \times \text{dispersion} \quad (6)$$

The results show that S_{ps} and S_p increase with increasing Zr content, so a critical factor in the isomerization selectivity of our synthesized catalysts is the platinum dispersion. The isomerization products were classified as two groups, monobranched (MOB) and multibranched (MUB) isomers. The molar ratio of multibranched to monobranched

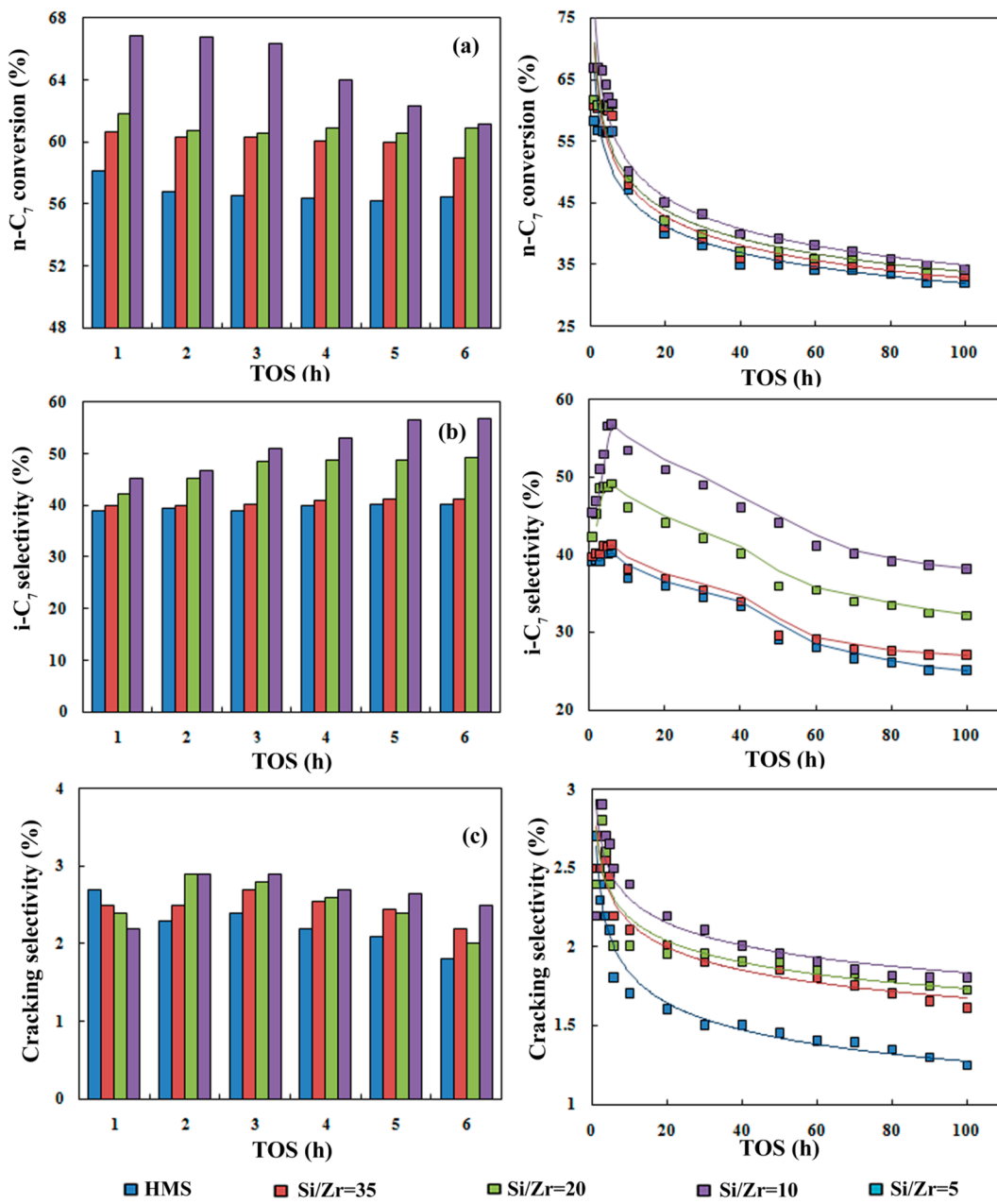


Figure 7. (a) n-C₇ conversion (%); (b) i-C₇ and (c) cracking selectivity versus time on stream (hours) over various catalysts at 400 °C.

isoheptanes (*R*) varies within a narrow range, between 0.7 and 1.0. MUB selectivity of our catalysts is much higher than that of other catalysts described in the literature.^{30,31} It is well-known that formation of the multibranched isomers would often be more difficult than that of the monobranched ones. Because the multibranched isoheptanes have larger molecular sizes, their formation, desorption, and diffusion inside the small pores would be hindered in most of the catalysts (such as zeolitic catalysts), which usually results in more cracking products. However, results showed that our catalysts have very good selectivity to MUB isomers, so the pore diameter of our synthesized catalysts plays a main role in multibranched C₇ formation.

These catalysts form very low aromatization products (between 0 and 3% selectivity), so we do not show them here. The mesoporous samples facilitate the hydrogen transfer reactions between olefinic and cyclic intermediates and so

enhance the yields of aromatics, cracking, and liquefied petroleum gas (LPG) products. It is well-known that the cracking and aromatization products increase with rising temperature. These reactions are competing reactions, and this competition is affected by the acidity, type of acid site, geometry, and balance between acid and metal functions. Aromatic compounds have relatively high octane numbers in a gasoline pool, but due to environmental regulations, at present, the production of reformulated gasoline with low content of benzene is one of the main purposes of the petrochemical industry.³² According to these results, our synthesized catalysts provide this goal and produce very low aromatization products.

We also compared our results with Pt/Al(5)-HMS catalyst (Figure 4). Pt/Al(5)-HMS shows better results due to higher acidity,⁵ and this behavior is not unexpected. This high acidity causes greater aromatic product selectivity (16.4–74% over the

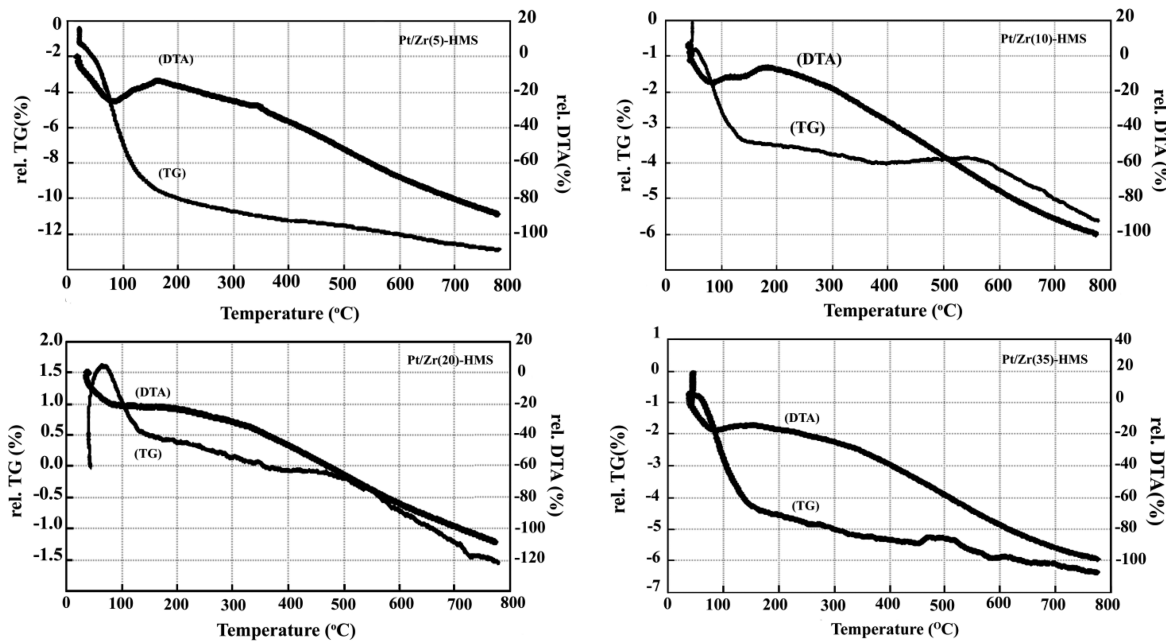


Figure 8. TG-DTA curves of the spent catalysts after 6 h.

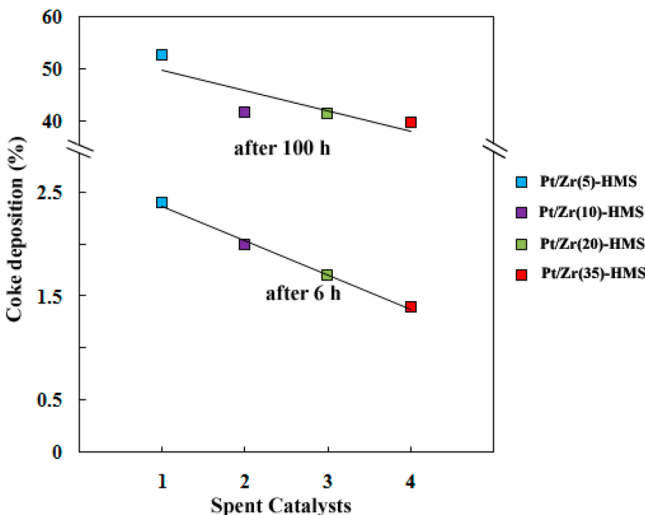


Figure 9. Amounts of coke deposited after 6 and 100 h during *n*-heptane conversion for various catalysts.

temperature range), and eventually coke formation (5.5%) and deactivation of the catalyst will be greater and faster.

Figure 6 presents RON of the reaction for each catalyst. To calculate RON, eq 7 was used:³³

$$\text{RON} = \sum_{i=1}^k y_i \text{RON}_i \quad (7)$$

RON is the measured octane number for total produced hydrocarbons after the reaction of *n*-C₇, whereas RON_i represents the pure-component octane number for each molecule *i* in the product, and *y_i* is the volume fractions of n-C₇ products.

As can be seen, Pt/Zr(5)-HMS compared to other catalysts, due to the production of molecules with higher RON_i, provides a higher octane number (RON). RON increases with increasing temperature. According to the results presented in the previous sections, RON results were not unexpected.

A problem that may arise with the use of hydrocarbons is poisoning of the catalyst. Hence, to investigate the coking study of these catalysts and catalytic stability in the range of reaction time, the experiments were continued for 100 h. The graphs of conversion, i-C₇, and cracking selectivity versus time on stream at 400 °C for all catalysts in 6 and 100 h on stream are given in Figure 7. Most changes in the reaction characteristics occur in the first 1–2 h on stream. The conversion of all catalysts decreases with increasing time on stream, but the decrease in the case of Pt/Zr(5)-HMS is more than those of other samples. Coke formation on these catalysts during the reaction confirms the conversion results. The carbon deposition over the spent catalysts after coking test was examined by TGA. The results of this analysis are given in Figure 8. As shown in this figure, the catalysts show a low weight loss. All catalysts show two weight losses in TGA curves. The weight losses at <150 °C, corresponding to endothermic peaks in DTA curves, were attributed to desorption of physically adsorbed water. The weight losses at >150 °C, corresponding to exothermic peaks in DTA curves, were ascribed to the combustion of carbonaceous material deposited inside used catalysts. The coke content on the spent catalysts are shown in Figure 9. This figure shows that coke deposition increases with increasing zirconium content. This greater amount of coke can be confirmed with higher deactivation and also with higher number of strong acid sites on Pt/Zr(5)-HMS. Also, these results suggest that the maximum amount of coke is laid down within the first 1–2 h on stream. The source of the coke is toluene or a toluene precursor molecule.³⁴ That, at the beginning of the reaction, is changed to cracking products and coke, but between 2 and 6 h on stream, the strong acid sites, responsible for cracking, are covered by coke, which is in agreement with increasing aromatic and isomer selectivity, as reported in the literature.^{35–37} After 6 h on stream, the selectivity of all catalysts reduces.

CONCLUSION

Corresponding to the results, the following conclusions can be drawn:

(i) The surface acidity is affected by the zirconium content. It is clearly observed that the acidity and strength of acid sites are directly related to the Zr content and increase almost linearly with Zr content (or decrease with increasing Si/Zr). The order of acidity is

$$\begin{aligned} \text{Zr(5)-HMS} &> \text{Zr(10)-HMS} \\ &> \text{Zr(20)-HMS} \\ &> \text{Zr(35)-HMS} \\ &> \text{HMS} \end{aligned}$$

(ii) The prepared catalysts have high conversion (31–100%), i-C₇ selectivity (28.6–64.1%), and low coke deposition (1.4–2.4) in reforming of n-heptane. High activity and selectivity for desirable products can be characteristic of porosity, acidity, and the nature of acid sites. This important result reveals the possibility to obtain high octane number gasoline by using Zr(x)-HMS-containing catalysts. Among these catalysts, Zr(5)-HMS has the best i-C₇ selectivity (64.1% at T = 200 °C). It can be seen that the order of activity and also selectivity of isomerization products is

$$\begin{aligned} \text{Zr(5)-HMS} &> \text{Zr(10)-HMS} \\ &> \text{Zr(20)-HMS} \\ &> \text{Zr(35)-HMS} \\ &> \text{HMS} \end{aligned}$$

which is in the same order as the increase in acidic site density.

(iii) The reaction kinetics measurements show that the rate of n-C₇ conversion under experiment conditions is controlled by the intrinsic reaction kinetics and is free from transport limitations, as determined from the Koros–Nowak and Madon–Boudart criteria. Activation energy was found to be 9.8–11.6 kJ/mol using Pt/Zr(x)-HMS catalysts, indicating that these catalysts have higher activity than HMS (E_a = 28.6 kJ/mol).

AUTHOR INFORMATION

Corresponding Author

*(M.H.P.) E-mail: m-peyrovi@sbu.ac.ir. Phone: +98 21 29902892. Fax: +98 21 22431663.

Notes

The authors declare no competing financial interest.

ACKNOWLEDGMENTS

We gratefully acknowledge financial support from the National Iranian Oil Refining and Distribution Co.

REFERENCES

- (1) Wang, J. A.; Zhou, X. L.; Chen, L. F.; Norena, L. E.; Yu, G. X.; Li, C. L. Hydroisomerization of n-heptane on the Pt/H₃PW₁₂O₄₀/Zr-MCM-41 catalysts. *J. Mol. Catal. A: Chem.* **2009**, *299*, 68.
- (2) Akhmedov, V. M.; Al-Khowaiter, S. H.; Al-Refai, J. K. Hydroconversion of C₅–C₈ alkanes over Zr-containing supported catalysts prepared by metal vapor method. *Appl. Catal. A: Gen.* **2003**, *252*, 353.
- (3) Yang, X.; Zhou, L.; Chen, Ch.; Xu, J. Synthesis of Zr-MCM-41 by the assistance of sodium chloride in the self-generated acid conditions. *Mater. Chem. Phys.* **2010**, *120*, 42.
- (4) Szczodrowski, K.; Prélét, B.; Lantenois, S.; Douillard, J. M.; Zajac, J. Effect of heteroatom doping on surface acidity and hydrophilicity of Al, Ti, Zr-doped mesoporous SBA-15. *Microporous Mesoporous Mater.* **2009**, *124*, 84.
- (5) Hamoule, T.; Peyrovi, M. H.; Rashidzadeh, M.; Toosi, M. R. Catalytic reforming of n-heptane over Pt/Al-HMS catalysts. *Catal. Commun.* **2011**, *16*, 234.
- (6) Chiranjeevi, T.; Kumaran, G. M.; Gupta, J. K.; Dhar, G. M. Synthesis and characterization of acidic properties of Al-HMS materials of varying Si/Al ratios. *Thermochim. Acta* **2006**, *443*, 87.
- (7) Zhang, Q.; Yang, W.; Wang, X.; Wang, Y.; Shishido, T.; Takehira, K. Coordination structures of vanadium and iron in MCM-41 and the catalytic properties in partial oxidation of methane. *Microporous Mesoporous Mater.* **2005**, *77*, 223.
- (8) Selvaraj, M.; Sinha, P. K.; Lee, K.; Ahn, I.; Pandurangan, A.; Lee, T. G. Synthesis and characterization of Mn–MCM-41 and Zr–Mn–MCM-41. *Microporous Mesoporous Mater.* **2005**, *78*, 139.
- (9) Gucbilmez, Y.; Dogu, T.; Balci, S. Vanadium incorporated high surface area MCM-41 catalysts. *Catal. Today* **2005**, *100*, 473.
- (10) Lim, S.; Yang, Y.; Ciuparu, D.; Wang, C.; Chen, Y.; Pfefferle, L.; Haller, G. L. The effect of synthesis solution pH on the physicochemical properties of Co substituted MCM-41. *Top. Catal.* **2005**, *34*, 31.
- (11) Igarashi, N.; Kidani, S.; Ahemaito, R.; Hashimoto, K.; Tatsumi, T. Direct organic functionalization of Ti–MCM-41: synthesis condition, organic content, and catalytic activity. *Microporous Mesoporous Mater.* **2005**, *81*, 97.
- (12) Lin, K.; Pescarmona, P. P.; Houthoofd, K.; Liang, D.; Tendeloo, G. V.; Jacobs, P. A. Direct room-temperature synthesis of methyl-functionalized Ti-MCM-41 nanoparticles and their catalytic performance in epoxidation. *J. Catal.* **2009**, *263*, 75.
- (13) Kong, Y.; Guo, X.; Zhang, F.; Jiang, S.; Wang, J.; Lu, Y.; Yan, Q. Synthesis of Ti-containing MCM41 using Ti(SO₄)₂ as Ti source. *Mater. Lett.* **2005**, *59*, 3099.
- (14) Occelli, M. L.; Biz, S.; Auroux, A. Effects of isomorphous substitution of Si with Ti and Zr in mesoporous silicates with the MCM-41 structure. *Appl. Catal. A: Gen.* **1999**, *183*, 231.
- (15) Gontier, S.; Tuel, A. Novel zirconium containing mesoporous silicas for oxidation reactions in the liquid phase. *Appl. Catal. A: Gen.* **1996**, *143*, 125.
- (16) Su, C.; Li, J.; He, D.; Cheng, Z.; Zhu, Q. Synthesis of isobutene from synthesis gas over nanosize zirconia catalysts. *Appl. Catal. A: Gen.* **2000**, *202*, 81.
- (17) Wu, Z. G.; Zhao, Y. X.; Liu, D. S. The synthesis and characterization of mesoporous silica–zirconia aerogels. *Microporous Mesoporous Mater.* **2004**, *68*, 127.
- (18) Zhang, Y. Q.; Wang, S. J.; Wang, J. W.; Lou, L. L.; Zhang, C.; Liu, S. Synthesis and characterization of Zr-SBA-15 supported tungsten oxide as a new mesoporous solid acid. *Solid State Sci.* **2009**, *11*, 1412.
- (19) Tanev, P. T.; Pinnavaia, T. J. A neutral templating route to mesoporous molecular sieves. *Science* **1995**, *267*, 865.
- (20) Kostova, N. G.; Spojakina, A. A.; Jiratova, K.; Solcova, O.; Dimitrov, L. D.; Petrov, L. A. Hexagonal mesoporous silicas with and without Zr as supports for HDS catalysts. *Catal. Today* **2001**, *65*, 217.
- (21) Ecormier, M. A.; Lee, A. F.; Wilson, K. High activity, templated mesoporous SO₄/ZrO₂/HMS catalysts with controlled acid site density for α-pinene isomerisation. *Microporous Mesoporous Mater.* **2005**, *80*, 301.
- (22) Chen, L. F.; Noreña, L. E.; Navarrete, J.; Wang, J. A. Improvement of surface acidity and structural regularity of Zr-modified mesoporous MCM-41. *Mater. Chem. Phys.* **2006**, *97*, 236.
- (23) Parry, E. P. An infrared study of pyridine adsorbed on acidic solids. Characterization of surface acidity. *J. Catal.* **1963**, *2*, 371.
- (24) Hughes, T. R.; White, H. M. A study of the surface structure of decationized Y zeolite by quantitative infrared spectroscopy. *J. Phys. Chem.* **1967**, *71*, 2192.
- (25) Liu, Y.; Guan, Y.; Li, C.; Lian, J.; Gan, G. J.; Lim, E. C.; Kooli, F. Effect of ZnO additives and acid treatment on catalytic performance of Pt/WO₃/ZrO₂ for n-C₇ hydroisomerization. *J. Catal.* **2006**, *244*, 17.

- (26) Koros, R. M.; Nowak, E. J. A diagnostic test of the kinetic regime in a packed bed reactor. *Chem. Eng. Sci.* **1967**, *22*, 470.
- (27) Madon, R. J.; Boudart, M. Experimental criterion for the absence of artifacts in the measurement of rates of heterogeneous catalytic reactions. *Ind. Eng. Chem. Fundam.* **1982**, *21*, 438.
- (28) Singh, U. K.; Vannice, M. A. Kinetics of liquid-phase hydrogenation reactions over supported metal catalysts – a review. *Appl. Catal. A: Gen.* **2001**, *213*, 1.
- (29) Kirumakki, S. R.; Nagaraju, N.; Chary, K. V. Esterification of alcohols with acetic acid over zeolites H β , HY and HZSMS. *Appl. Catal. A: Gen.* **2006**, *299*, 185.
- (30) Pope, T. D.; Kriz, J. F.; Stanculescu, M.; Monnier, J. A study of catalyst formulations for isomerization of C₇ hydrocarbons. *Appl. Catal. A: Gen.* **2002**, *233*, 45.
- (31) Kinger, G.; Majda, D.; Vinek, H. n-Heptane hydroisomerization over Pt-containing mixtures of zeolites with inert materials. *Appl. Catal. A: Gen.* **2002**, *225*, 301.
- (32) Roy, S.; Datta, S. Hydrogenation of toluene on zirconium-modified hexagonal molecular sieve supported platinum and palladium catalysts. *Ind. Eng. Chem. Res.* **2013**, *52*, 17360.
- (33) Nikolaou, N.; Papadopoulos, C. E.; Gaglias, I. A.; Pitarakis, K. G. A new non-linear calculation method of isomerisation gasoline research octane number based on gas chromatographic data. *Fuel* **2004**, *83*, 517.
- (34) Peyrovi, M. H.; Hamoule, T. Study of catalytic properties of Pt/Al-HMS catalysts in n-heptane hydroisomerization. *React. Kinet. Mech. Catal.* **2012**, *106*, 233.
- (35) Bowker, M.; Aslam, T.; Roebuck, M.; Moser, M. The effect of coke lay-down on n-heptane reforming on Pt and Pt-Sn catalysts. *Appl. Catal. A: Gen.* **2004**, *257*, 57.
- (36) Yang, X.; Liao, S.; Zeng, J.; Liang, Z. A mesoporous hollow silica sphere (MHSS): synthesis through a facile emulsion approach and application of support for high performance Pd/MHSS catalyst for phenol hydrogenation. *Appl. Surf. Sci.* **2011**, *257*, 4472.
- (37) Posada, J. A.; Cardona, C. A.; Giraldo, O. Comparison of acid sulfonic mesostructured silicas for 1-butylacetate synthesis. *Mater. Chem. Phys.* **2010**, *121*, 215.